Model-informed design of antibiotic therapy against antimicrobial resistance

Tandar, S.T.

Chapter 3

Semi-mechanistic modeling of resistance development to β-lactam and β-lactamase-inhibitor combinations

Sebastian T. Tandar
Linda B. S. Aulin
Eva M. J. Leemkuil
Apostolos Liakopoulos
J. G. Coen van Hasselt

Journal of Pharmacokinetics and Pharmacodynamics (2024) 51(3):199–211.

Abstract

The use of β-lactam (BL) and β-lactamase inhibitor (BLI) combinations, such as the piperacillin and tazobactam combination (PIP-TAZ), is an effective strategy to combat infections by extended-spectrum β-lactamase-producing bacteria. However, in Gram-negative bacteria, resistance (both mutational and adaptive) to BL-BLI combination can still develop through multiple mechanisms. These mechanisms may include increased β-lactamase activity, reduced drug influx, and increased drug efflux. Understanding the relative contribution of these mechanisms during resistance development helps identify the most impactful mechanism to target in designing a treatment to counter BL-BLI resistance. This study used semi-mechanistic mathematical modeling in combination with antibiotic sensitivity assays to assess the potential impact of different resistance mechanisms during the development of PIP-TAZ resistance in a *Klebsiella pneumoniae* isolate expressing CTX-M-15 and SHV-1 β-lactamases. The mathematical models were used to evaluate the potential impact of several cellular changes as a sole mediator of PIP-TAZ resistance. Our semi-mechanistic model identified 2 out of the 13 inspected mechanisms as key resistance mechanisms that may independently support the observed magnitude of PIP-TAZ resistance, namely porin loss and efflux pump up-regulation. Simulation using the resulting models also suggested the possible adjustment of PIP-TAZ dose outside its commonly used 8:1 dosing ratio. The current study demonstrated how theory-based mechanistic models informed by experimental data can be used to support hypothesis generation regarding potential resistance mechanisms, which may guide subsequent experimental studies.

Introduction

Antimicrobial resistance in Gram-negative bacteria poses a threat to public health[1]. One of the concerns is associated with the expression of extended spectrum β-lactamases (ESBLs), which confers antibiotic resistance to beta-lactams (BLs)[2], a cornerstone antibiotic class to treat Gram-negative infections. BL-type antibiotics exert its bactericidal effect by inhibiting the activity of penicillin-binding proteins (PBPs) in the periplasm. One treatment strategy against ESBL-producing strains is the co-administration of β-lactamase inhibitors (beta-lactamase inhibitors (BLIs)) alongside BL-antibiotics[3]. BLIs lack bactericidal activity on their own but protect the co-administered BL antibiotic from degradation by β-lactamases[3,4]. Piperacillin-tazobactam (PIP-TAZ) is a commonly used BL-BLI combination that is mainly prescribed for the treatment of Gram-negative bacterial infections[4].

Despite the success of PIP-TAZ combination, resistance against this combination has been reported[5,6]. In this study, the term 'resistance' is used to generally describe the decrease in antibiotic sensitivity observed as changes on bacterial population growth rate without distinguishing the mutational or adaptive nature of its development. In Gram-negative bacteria, resistance to BL-BLI combination is mainly achieved through elevated β-lactamase activity[7], reduced drug influx through the outer membrane[8], or increased drug efflux[8,9] (**Fig. 1**). These resistance mechanisms may decrease the effective BL concentration in the periplasm, thereby reducing the bactericidal effect exerted on the bacteria[10]. Although these mechanisms may simultaneously contribute to promoting PIP-TAZ resistance, assessing the potential importance of each individual mechanism may allow guide the rational design of treatments countering emergence of resistance.

Comprehensive quantitative assessment of the relative contribution of potential resistance mechanisms is a complex task. While the effect of a specific resistance mechanism can be targeted by experimental assays[11–13], conclusion drawn from such observations may be convoluted by the concurrence of multiple resistance mechanisms. Unlike experimental assays, semi-mechanistic mathematical models representing the transfer and effect of antibiotics can be adjusted freely to highlight the effect of one (set of) cellular change towards antimicrobial resistance. This allows mathematical models to be used as a hypothesis-generating tool to identify key antibiotic resistance mechanism(s) based on prior knowledge[14,15]. The primary objective of this study was to showcase the utility of semi-mechanistic models as a means of theoretical exploration to understand the potential impact of different cellular mechanisms that may mediate PIP-TAZ resistance and subsequently help identify cellular mechanisms that may be prioritized in future studies. Additionally, we demonstrated how a semi-mechanistic may be used as a supplementary tool to support the design of antibiotic treatment against resistance.

Methods

Bacterial strain and culture condition

The current study focused on *Klebsiella pneumoniae* isolate GR116.26, which harbored a genomic copy of *blaCTX-M-15* and *blaSHV-1* β-lactamase genes[16]. *blaSHV-1* β-lactamase was generally expected from most *K. pneumoniae* strains[16]. All liquid cultures were carried out in cation-adjusted Mueller-Hinton (MH) broth (Becton Dickinson) and were incubated at 37°C.

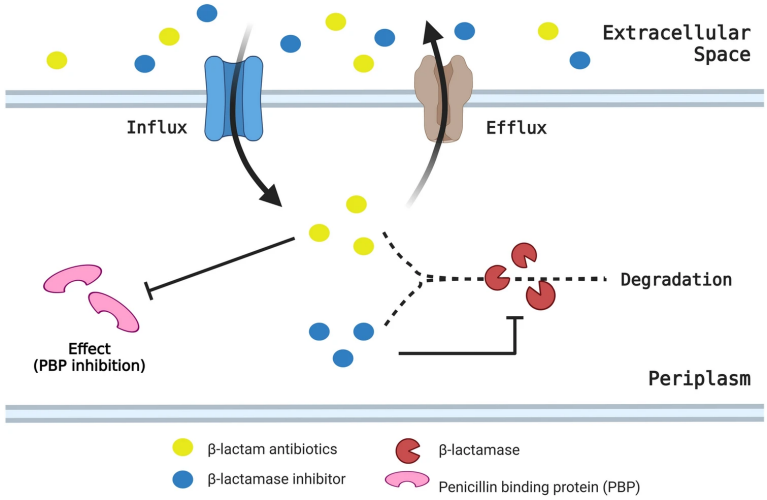

Fig. 1 | Periplasmic mass transfer and activity of PIP-TAZ in gram-negative bacteria. PIP-TAZ transfer and bactericidal effect in the periplasmic space. Periplasmic (*pp*) accumulation of PIP and TAZ are determined by their influx, efflux, and degradation. Bactericidal effect through PBP inhibition was assumed to be a function of periplasmic PIP concentration and was empirically expressed using the Hill equation. Pointed arrows represented mass transfer through the outer membrane, dashed lines represent degradation, and blunt arrow represent inhibitory activity

Antibiotic sensitivity assays

Checkerboard assays were performed to approximate PIP and TAZ concentration ranges to be included in the main static time-kill (STK) assay. Checkerboard assays were carried out on a in 96-well plates (Greiner Bio-One, flat bottom, 200 μL culture scale with 200 rpm orbital shaking). The checkerboard assay included 66 PIP-TAZ concentration combinations with PIP and TAZ concentrations ranging from 0 to 256 mg/L and 0 to 16 mg/L, respectively (Fig. S2). Bacterial growth was monitored by optical density at 600 nm (OD_{600}; BMG Fluostar Omega).

STK assays were performed to characterize the pharmacodynamics of PIP-TAZ combination. STK assays were carried out on a 20 mL scale with 150 rpm linear shaking. This assay included 17 PIP-TAZ concentrations ranging from 0 to 16 mg/L and 0 to 256 mg/L for PIP and TAZ, respectively. These concentrations were selected based on the result of the preceding checkerboard assay. STKSTK cultures were sampled (500 μL) at 0, 1, 2, 3, 4, 5, 6, 7, 24, and 48 hours after the inoculation, giving an end volume of approximately 15 mL. Serial dilutions (10-fold dilution at each dilution steps) were performed using 0.9% (w/v) drug-free NaCl solution to achieve a final colony count of 20–200 colonies on the agar plate. Undiluted samples were also plated when low cell density was expected. The samples were not subjected to antibiotic removal (cell washing) prior to dilution and/or plating to mitigate potential cell loss, particularly in samples with low cell density. Consequently, there may have been antibiotic carryovers in less diluted samples. 50 μL of the resulting (un)diluted sample on drug-free MH agar plates (VWR™ MH and APC Pure bacteriological agar) using Whitley Automatic Spiral Plater with Vacuum Source 602 for colony forming units (CFU) measurement (400 CFU/mL lower limit of quantification; LLoQ). Both assays were performed with a starting inocu-

lum of approximately 10^6 CFU/mL. Drugs were added to the culture medium before inoculation. Assays were performed in triplicates.

Model structure

PIP-TAZ mass transfer. Porin-mediated import of PIP-TAZ across the bacterial outer membrane was assumed to follow passive diffusion (**Eq. 1**)[10,17]. Here, P and A represent membrane permeability and surface area, respectively. The transfer was assumed to be driven by concentration gradient between the external/assay drug concentration (C_{ext}) and the periplasmic drug concentration (C_{pp}). Porin was assumed to act as passive transport mediator. Porin expression is thus assumed to be linearly correlated to membrane permeability ($P \propto porin$).

$$\left(\frac{dC_{\mathrm{pp}}}{dt}\right)_{\mathrm{import}} = P \times A \times (C_{\mathrm{ext}} - C_{\mathrm{pp}}) \qquad \textbf{Eq. 1}$$

PIP-TAZ efflux by the efflux pumps was described using the Michaelis-Menten equation adjusted for cooperativity[18] (**Eq. 2**). Here, PIP-TAZ efflux rate was expressed using $V_{efflux,max}$, K_{efflux}, and h, which represent the maximum rate of efflux, drug-efflux pump binding coefficient, and Hill exponent, respectively. Since the equation was derived from the Michaelis-Menten kinetics, $V_{efflux,max}$ was assumed to be proportional to efflux pump expression.

$$\left(\frac{dC_{\mathrm{pp}}}{dt}\right)_{\mathrm{efflux}} = -V_{\mathrm{efflux,max}} \times \frac{C_{\mathrm{pp}}^{h}}{C_{\mathrm{pp}}^{h} + K_{\mathrm{efflux}}^{h}} \qquad \textbf{Eq. 2}$$

Drug hydrolysis by β-lactamases was modeled using the Michaelis-Menten equation[19,20] (**Eq. 3**), where $k_{cat,Enzyme}$, and K_m represent the catalytic rate of the β-lactamases towards the substrate, enzyme concentration, and Michaelis constant of the β-lactamases towards the respective drug[19].

$$\left(\frac{dC_{\mathrm{pp}}}{dt}\right)_{\mathrm{hydrolysis}} = -k_{\mathrm{cat}} \times [\mathrm{Enzyme}] \times \frac{C_{\mathrm{pp}}}{C_{\mathrm{pp}} + K_{\mathrm{m}}} \qquad \textbf{Eq. 3}$$

PIP-TAZ binding competition to β-lactamases and efflux pumps. The kinetics of PIP and TAZ binding to β-lactamases and efflux pumps were assumed to be competitive and reversible[19]. The effect of the competitive binding was reflected on the parameters K_{efflux} and K_m. Here, we assumed that only a single PIP or TAZ molecule can interact with one β-lactamase or efflux pump at a time. The effective value ($K_{effective}$) of these constants in the presence of the competitor at the periplasm ($C_{pp,competitor}$) is expressed by **Eq. 4**, where K represents the binding constant of the molecule of interest and Kcompetitor represents the binding constant of the competitor molecule[19].

$$K_{\mathrm{effective}} = K \times \left(1 + \frac{C_{\mathrm{pp,competitor}}}{K_{\mathrm{competitor}}}\right) \qquad \textbf{Eq. 4}$$

Periplasmic β-lactamase availability. The availability of CTX-M-15 and SHV-1 β-lactamases in the periplasm were described by its background expression level R_0 and

its natural degradation rate k_{deg}. The value of k_{deg} was fixed to 0.01 (h^{-1}), as previously reported for most proteins in Gram-negative bacteria[21]. Additionally, TAZ degradation was assumed to inactivate the associated β-lactamase (suicide inhibition)[22].

$$\frac{d[\text{Enzyme}]}{dt} = R_0 \times k_{\text{deg}} - [\text{Enzyme}] \times k_{\text{deg}} + \left(\frac{dC_{\text{TAZ,pp}}}{dt}\right)_{\text{hydrolysis}} \quad \textbf{Eq. 5}$$

Eq. 5 infers that in the absence of TAZ, Image will be reached at the steady state. In the current study, the units of R_0 were kept as arbitrary unit to account for the differences in enzyme concentrations used in the assays reported in the reference studies[19,20]. Absolute values of β-lactamase concentrations can be derived by multiplying the simulated enzyme units with the concentration of β-lactamase used in the referenced experiments for the specific β-lactamase.

Bacterial growth and bactericidal effects. The growth of a bacterial population (N) was described using the population-limited growth model with system carrying capacity of N_{max}. The effective (observed) growth rate of the bacterial population was assumed to be the sum of its natural growth rate (k_{growth}) and the effective kill rate (bactericidal effect) from being exposed to antibiotics (**Eq. 6**).

$$\frac{dN}{dt} = k_{\text{growth}} \times N \times \left(1 - \frac{N}{N_{\text{max}}}\right) - E \times N \quad \textbf{Eq. 6}$$

The bactericidal effect exerted on the population as effective kill rate was represented as a function of the periplasmic concentration of PIP (the bactericidal agent). A Hill equation was selected as an empirical description for PIP bactericidal effect on the bacterial growth (**Eq. 7**), where E_{max}, EC_{50}, and H represent the maximum bactericidal effect, the PIP concentration required to achieve half-maximum kill rate, and the Hill exponent, respectively. The bactericidal effect of TAZ was negligible (Fig. S2)[4].

$$E = E_{\text{max}} \times \frac{C_{\text{PIP,pp}}^{H}}{C_{\text{PIP,pp}}^{H} + EC_{50}^{H}} \quad \textbf{Eq. 7}$$

The development of resistance. The initial PIP-TAZ pharmacodynamics (before the point of regrowth) was described using a one-population model (Fig. S1a). In a one-population model, the bacterial population was assumed to consist of only a single population which shared the same growth and drug sensitivity characteristics.

The STK assays allow merely phenotypic observation of resistance development (regrowth). Semi-mechanistic models were used to derive mechanistic understanding from such phenotypic observation. Here, a two-population growth model[23] was used to describe the development of resistance (Fig. S1b). This model assumed the presence of a susceptible (N_S) and a less sensitive or resistant (N_R) bacterial population. The bacterial population was assumed to be fully susceptible at the start of the experiment. A first-order transfer rate ($k_{trasnfer}$) was used to empirically describe the transition of susceptible (N_S) into resistant (N_R) bacteria. The drug effect exerted on the susceptible and resistant bacterial population was denoted by E_S and E_R, respectively. In the two-population growth models, the effective growth rates of both populations were determined by the sum of its growth, bactericidal effect that it experienced, and its susceptible-to-resistance transition (**Eq. 8** and **Eq. 9**).

$$\frac{dN_S}{dt} = k_{\text{growth}} \times N_S \times \left(1 - \frac{N_S + N_R}{N_{\max}}\right) - E_S \times N_S - k_{\text{transfer}} \times N_S \qquad \textbf{Eq. 8}$$

$$\frac{dN_R}{dt} = k_{\text{growth}} \times N_R \times \left(1 - \frac{N_S + N_R}{N_{\max}}\right) - E_R \times N_R + k_{\text{transfer}} \times N_S \qquad \textbf{Eq. 9}$$

In each model, the resistant population was assumed to possess a single mechanism of resistance. This resistance mechanism was depicted in the model as changes in one of its resistance-associated parameters (**Eq. 10**). Here, the value of a specific resistance-associated parameter was in the resistant bacterial sub-population ($Parameter_{resistant}$) was assumed to be higher or lower than that of the susceptible bacterial sub-population ($Parameter_{susceptible}$) with a factor of α. These resistance-associated parameters represented one of 13 parameters including outer membrane permeability, maximum efflux rate, efflux pump binding constant, β-lactamase expression level (CTX-M-15 and SHV-1), CTX-M-15 catalytic rate and Michaelis constant for PIP and TAZ, and SHV-1 catalytic rate and Michaelis constant for PIP and TAZ.

$$Parameter_{resistant} = \alpha \times Parameter_{susceptible} \qquad \textbf{Eq. 10}$$

Source of model parameters

Experimentally determined kinetic PIP-TAZ parameters were fixed to reported values (**Table 1**). Parameters related to strain growth (k_{growth}, N_{max}, inoculum size), drug effect (E_{max}, EC_{50}, H), and resistance development ($k_{transfer}$, α) were empirically fitted to experimental observations. At the time of the study, TAZ influx and efflux parameters were not available. The values of TAZ influx and efflux parameters were thus fixed to that of PIP. This decision was justified based on the knowledge that the permeability coefficient and maximum efflux rate across eight different β-lactams showed variation only within the same order of magnitude[18] (Table. S2). The assumptions made during the model development process are summarized on the supplementary Table S1.

Model parameter fitting

Mixed-effect model development and simulation were performed using 'nlmixr2' (v.2.0.7) and 'rxode2' (v.2.0.7) packages in R (v.4.2.1). Mixed-effect models included a random effect term on inoculum size to account for possible variability related to the inoculation step. Initial estimates for model fitting routines were determined using particle swarm optimization (PSO; 'pso' package; v.1.0.3). Parameter fitting was performed based on STK assay observation. CFU measurements with values below the LLoQ (400 CFU/mL) were replaced with LLoQ/2.

Model parameters were fitted sequentially to prevent identifiability issues. The values for k_{growth} and N_{max} were estimated based on observation from the no-drug control and were fixed in subsequent model fitting steps. Drug effect parameters were fitted from observations made in the first 5-hours of the experiment using the one-population model and were fixed in two-population models. Parameters related to resistance were fitted using the full 48-hours observation data.

Resistance mechanism evaluation

Two-population models (Fig. S1b) were used to assess the extent of cellular changes required for a specific resistance mechanism to describe the observed regrowth in our STK experiment. Here, PIP-TAZ resistance in the resistant sub-population was depicted as a change in one of the 13 resistance mechanism-associated parameters. Resistance mechanisms were thus individually represented in 13 semi-mechanistic models. By fitting the models to experimental observations, we estimated the extent of cellular changes (represented as α on **Eq. 10**) required by the initial susceptible population to show the observed level of resistance. The physiological feasibility of each resistance mechanism was then evaluated by comparing the extent of cellular changes estimated by our model to the extent of cellular changes reported for a resistant strain with respect to a susceptible strain of reference.

Table 1. Literature-based PIP-TAZ transport parameters.

Parameters	**Value**	**Units**	**References**
PIP outer membrane permeability coefficient (P_{PIP})	3.67×10^{-5}	cm/s	[18] (mean)
Cell surface area (A)	132	cm^2/mg-cell	[18]
CTX-M-15 specific PIP hydrolysis rate ($k_{\mathrm{cat,PIP,CTX\text{-}M\text{-}15}}$)*	58	s^{-1}	[19]
CTX-M-15 Michaelis constant to PIP ($K_{\mathrm{m,PIP,CTX\text{-}M\text{-}15}}$)*	32	μM	[19]
CTX-M-15 specific TAZ hydrolysis rate ($k_{\mathrm{cat,TAZ,CTX\text{-}M\text{-}15}}$)*	5.70×10^{-3}	s^{-1}	[19]
CTX-M-15 Michaelis constant to TAZ ($K_{\mathrm{m,TAZ,CTX\text{-}M\text{-}15}}$)*	1.70×10^{-2}	μM	[19]
SHV-1 specific PIP hydrolysis rate ($k_{\mathrm{cat,PIP,SHV\text{-}1}}$)	86	s^{-1}	[20]
SHV-1 Michaelis constant to PIP ($K_{\mathrm{m,PIP,SHV\text{-}1}}$)	91	μM	[20]
SHV-1 specific TAZ hydrolysis rate ($k_{\mathrm{cat,TAZ,SHV\text{-}1}}$)	0.1	s^{-1}	[20]
SHV-1 Michaelis constant to TAZ ($K_{\mathrm{m,TAZ,SHV\text{-}1}}$)	7.00×10^{-2}	μM	[20]
PIP maximum efflux rate ($V_{\mathrm{efflux,max,PIP}}$)	3.77×10^{-1}	nmol mg-cell^{-1} s^{-1}	[18]
PIP concentration for half-maximum efflux ($K_{\mathrm{efflux,PIP}}$)	1.07	μM	[18]
PIP efflux Hill coefficient (h)	3.97		[18]
Protein (β-lactam) turnover rate ($k_{\mathrm{degradation}}$)	0.01	h^{-1}	[21]

* Periplasmic transport parameters were measured in or with protein derived from *Escherichia coli*, except for those marked with (*), which were derived from *Enterobacter cloacae*-derived CTX-M-15 β-lactamase.

Growth inhibition simulation

Model simulations were performed to explore how specific resistance mechanisms may influence the survivability of the strain in different PIP-TAZ concentrations. The current simulation was also used to evaluate the potential of PIP-TAZ dose adjustment to counter a specific resistance mechanism. This analysis was performed using the porin

down-regulation and efflux pump up-regulation. Simulation was performed using a starting inoculum size of 10^5 CFU/mL and included PIP-TAZ concentration ranges of 1 to 512 mg/L and 0.125 to 512 mg/L for PIP and TAZ, respectively. Each PIP-TAZ concentration combination was evaluated based on the bacterial density at the 24th hour of the culture predicted by the three models. For this analysis, we considered bacterial growth to be suppressed if the simulated cell density at the 24th hour was less than the inoculum size.

Parameter sensitivity analysis

Parameter sensitivity analysis was performed to investigate the impact of deviations in literature-based parameters. The sensitivity analysis focused on four selected PIP-TAZ concentrations, specifically 0-0, 4-2, 16-4, and 256-16 mg/L PIP-TAZ, to cover concentrations where different magnitudes of initial bactericidal effects were observed. Absolute sensitivity coefficients ($S_{absolute}$) were derived from the absolute value of the ratio of the shift in total bacterial load (L; the area under the bacterial growth curve) relative to the shift in the value of a specific parameter of interest, denoted by β (**Eq. 11**). The ratios of parameter shift investigated in the analysis ranged from 0.25 to 1.75, with increments of 0.25.

$$S_{\text{absolute}} = \frac{L/L_{\text{original}}}{\beta/\beta_{\text{original}}} \qquad \textbf{Eq. 11}$$

Results

Preliminary description of PIP-TAZ pharmacodynamics

Our study used STK assays to investigate the behavior of a CTX-M-15-producing *K. pneumoniae* strain GR116.26 in different concentrations of PIP-TAZ. From this experiment, we could see how the presence of both PIP and TAZ was required to achieve an initial population decline. In the presence of both PIP and TAZ, increasing PIP and/or TAZ concentrations resulted in a higher bactericidal effect as seen by the initial population decline observed at higher PIP-TAZ concentrations (Fig. S3). Even though an initial population decline was observed in some PIP-TAZ concentrations, in most cases, the population was able to regrow at approximately 5 hours after inoculation (Fig. S3; grey lines). Given the timeframe of the observed regrowth and the stability of PIP and TAZ over 24 hours[24,25], it was likely that the observed regrowth was due to the development of resistance – as indicated by the apparent decrease in observed PIP-TAZ bactericidal activity.

One-population model was used to describe the behavior of the strain in different PIP-TAZ concentrations before the onset of regrowth (**Table 2**, Fig. S4). This initial model demonstrated the impact of TAZ on the concentration-effect curve of PIP-TAZ (**Fig. 2**; Fig. S5). As illustrated in **Fig. 2**, an increase in TAZ concentration could achieve a bactericidal effect equal to the natural growth rate of the strain (indicated by the red dashed line) with a lower concentration of PIP. Additionally, this model can be used to simulate how changes in a specific resistance mechanism may impact the effect of PIP-TAZ on bacterial growth. Here, we simulated how changes in the values of 13 resistance mechanism-associated parameter may impact effective antibiotic kill rate at 16-4 mg/L PIP-TAZ concentration (**Fig. 2b**).

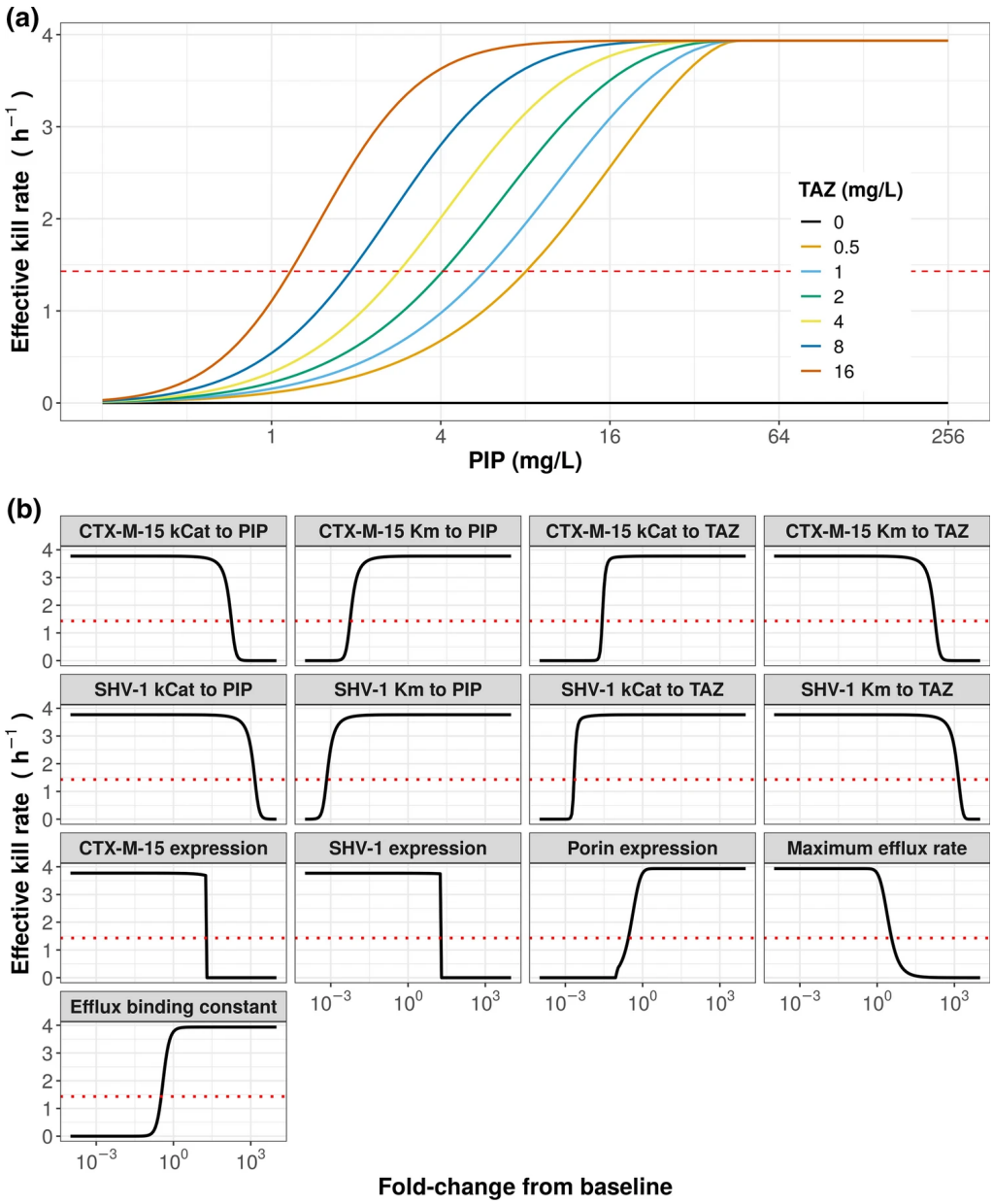

Fig. 2 | Preliminary assessment of initial PIP-TAZ exposure-response characteristics on *K. pneumoniae* GR112.6. The initial PIP-TAZ pharmacodynamics on the tested strain was evaluated before the onset of regrowth. The assessment was performed using a one-population model and was based on experimental observations during the first 5 h of the culture. (a) Simulation using the one-population model described how increasing TAZ concentration allowed a higher bactericidal effect to be reached at a lower extracellular PIP concentration. Dashed red line denotes the natural growth rate. (b) The capacity of each resistance mechanism to allow strain survival in 16-4 mg/L PIP-TAZ. Dashed red lines represent the natural growth rate.

Table 2. One-population model estimates for growth and PIP–TAZ pharmacodynamics.

Parameters	Value (95% CI)	Units
Natural growth rate[a]	1.43 (1.23–1.67)	h^{-1}
Maximum population size[a]	1.36×10^9 (8.94×10^8–2.08×10^9)	CFU/mL
Baseline β-lactamase level (R_0)	1.36×10^5 (1.33×10^5–1.39×10^5)	μM
Inoculum size	8.01×10^5 (8.00×10^5–8.01×10^5)	CFU/mL
Maximum bactericidal effect (E_{max})	3.93 (3.92–3.95)	h^{-1}
Intracellular PIP concentration for half-maximum bactericidal effect (EC_{50})	1.44 (1.43–1.44)	μM
Hill exponent of bactericidal effect (H)	3.82 (3.81–3.84)	–

[a] Parameter value predicted based on observations made in the absence of PIP–TAZ.

Model-based assessment of resistance mechanisms

The following analysis aimed to predict and assess the magnitude of changes required to convey resistance to the observed PIP-TAZ concentrations. The current analysis included 13 models, each depicting one of the thirteen potential mechanisms evaluated in the current study (**Fig. 2b**). Our models predicted the extent of cellular changes required for the strain to achieve the observed level of PIP-TAZ resistance (**Fig. 2**; **Table 3**; Fig. S6).

The obtained model estimates were compared with literature reports to assess the physiological feasibility of each mechanism to serve as a single mediator of PIP-TAZ resistance. This was then followed by the selection of resistance mechanisms that required changes that were less extreme than that reported in the literature (**Table 3**). Based on this analysis, 8 out of the 13 resistance mechanisms were predicted to require cellular changes that were more extreme than what was previously reported for the mechanism. For example, our model predicted that an 8.93×10^4-fold CTX-M-15 up-regulation was needed for the hydrolysis of PIP in the presence of the TAZ to confer the observed levels of PIP-TAZ resistance seen in our STK by this mechanism. This value was more than 100-fold higher than the maximum extent of β-lactamase up-regulation reported in the literature (up to 300-fold up-regulation compared to the expression level of the strain of reference; **Table 3**), making CTX-M-15 up-regulation an unlikely single-event mechanism mediating the PIP-TAZ resistance observed in our experiment. 3 out of the 13 resistance mechanisms, namely decreased TAZ catalytic rate by SHV-1 and CTX-M-15 β-lactamases as well as increased drug affinity to efflux pumps were excluded due to the lack of experimental evidence of its occurrence in the literature, even though our analysis showed that either of these mechanisms can potentially serve as a single-mechanism mediator to PIP-TAZ resistance.

Two of the mechanisms evaluated in this study could promote PIP-TAZ resistance without requiring cellular changes that were more extreme than what was reported in the literature (**Table 2**; **Fig. 3**). The first mechanism identified in our workflow was the reduction of PIP-TAZ permeability through the outer membrane, leading to decreased intracellular concentrations of PIP and/or TAZ. A decrease in PIP-TAZ permeability predicted by our model (9.36×10^{-2}-fold decrease compared to the initial susceptible

Table 3. Fold parameter change required to describe the observed PIP-TAZ resistance

Affected parameter	Physiological relevance	Magnitude (fold-change)	Magnitude observed in the literature
Outer membrane permeability (P)	Porin loss/reduced porin permeability	9.63×10^{-2}	Down-regulation or complete inactivation of OmpK35/36[26;a]
Maximum efflux rate ($V_{\text{efflux,max}}$)	Increased efflux pump expression/increased maximum efflux rate	2.15×10^{1}	*oqxB, rarA, acrA, ketM, kdeA, kpnF*, and *kexD* up-regulation; up to 1.08×10^{3}-fold[27;b]
Efflux pump binding constant (K_{efflux})	Increased PIP-TAZ affinity to efflux pumps	2.00×10^{-2}	No previous report found.
Baseline CTX-M-15 level ($R_{0,\text{CTX-M-15}}$)	Increased β-lactamase level	8.93×10^{4}	β-lactamase up-regulation within 10-300-fold[28,29]
Baseline SHV-1 level ($R_{0,\text{SHV-1}}$)		1.02×10^{4}	
CTX-M-15 PIP catalytic rate ($k_{\text{cat,CTX-M-15,PIP}}$)	Increased PIP hydrolysis rate	2.97×10^{5}	TEM mutants may increase catalytic rate to a specific compound by up to 515-fold[30;c]
SHV-1 PIP catalytic rate ($k_{\text{cat,SHV-1,PIP}}$)		7.29×10^{5}	
CTX-M-15 TAZ catalytic rate ($k_{\text{cat,CTX-M-15,TAZ}}$)	Decreased TAZ hydrolysis rate	1.37×10^{-6}	No previous report found.
SHV-1 TAZ catalytic rate ($k_{\text{cat,SHV-1,TAZ}}$)		3.05×10^{-6}	
CTX-M-15 PIP Michaelis constant ($K_{\text{m,CTX-M-15,PIP}}$)	Increased β-lactamase affinity to PIP	1.61×10^{-2}	Decrease in K_m values by approximately 0.5-fold in SHV-1 against several β-lactams[31]
SHV-1 PIP Michaelis constant ($K_{\text{m,SHV-1,PIP}}$)		8.29×10^{-2}	
CTX-M-15 TAZ Michaelis constant ($K_{\text{m,CTX-M-15,TAZ}}$)	Reduced β-lactamase affinity to TAZ	2.57×10^{3}	Up to 60-fold increase in SHV-1 K_m to TAZ[20]
SHV-1 TAZ Michaelis constant ($K_{\text{m,SHV-1,TAZ}}$)		3.63×10^{4}	

[a] May be associated with the up-regulation of other porin subtypes.
[b] May be associated with the down-regulation of other efflux pump(s).
[c] Evolutionary tradeoff may lower hydrolysis rate of other β-lactams.

population) can be achieved by down-regulation or loss of porins, the proteins that facilitate PIP-TAZ entry into the periplasm[17,26]. A previous study supported our model prediction by highlighting the role of OmpK[32] porin in facilitating BL transport into *K. pneumoniae* cells and by further revealing the central role of its deletion in the development of BL resistance[33]. The second mechanism highlighted in our workflow was the 21.5-fold increase in efflux pump activity in the resistant population compared to that of the initial susceptible population. Increased efflux pump activity is often mediated by up-regulation of one or more efflux pumps. In *K. pneumoniae*, the up-regulation of *oqxA, kexD, kpnF,* and *acrB* efflux pumps were observed in isolates showing different ranges of β-lactam resistance[34]. Overall, the current workflow identified reduction of drug influx and increased efflux pump activity as mechanisms that may independently mediate PIP-TAZ resistance to the level that was observed in our experimental setting.

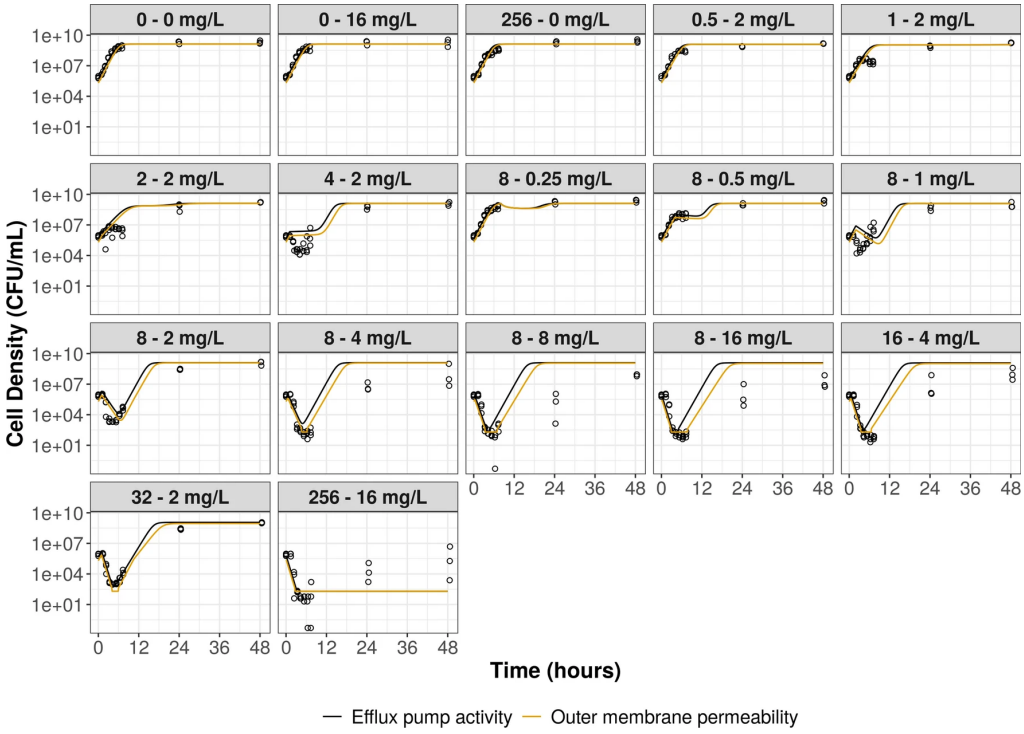

Fig. 3 | Observed and predicted population growth dynamics under porin down-regulation and efflux pump up-regulation. Population growth prediction using porin down-regulation and efflux pump up-regulation models. Data points represented individual observation obtained during the STK experiment. Lines represented the typical prediction performed using the efflux pump up-regulation model (efflux pump activity) and porin down-regulation model (outer membrane permeability). Drug concentrations were presented in the following format: PIP concentration-TAZ concentration (mg/L).

Both porin down-regulation and efflux pump up-regulation models overestimated population growth at PIP-TAZ concentrations of 8-4, 8-8, 8-16, and 16-4 mg/L while under-estimated the regrowth at 256-16 mg/L. These deviations could be caused by the application of first-order kinetics used to describe the development of resistance in our models. This implied that our models are constrained to the characterization of

resistance as a unimodal process, whereas, in reality, the development of resistance could potentially encompass a complex, multi-stage mechanism. The disagreement between observation and model prediction at these concentration ranges may also be rooted in the use of literature-based parameters that were derived from a different bacterial strain and/or species. To further investigate the issue, a parameter sensitivity analysis was conducted to evaluate the model parameters' influence on the model prediction. The analysis indicated the relatively higher sensitivity of the model estimates towards PIP-TAZ influx and efflux parameters compared to other literature-based parameters used in our models (Fig. S7). While the current parameter sets represented the best available information for the present study, future studies are suggested to characterize these parameters to represent the PIP-TAZ influx and efflux more accurately in the model, thereby improving the predictive capability of the models.

In this study, we substituted measurement observations below the limit of quantification (BLoQ) with LLoQ/2. This method of BLoQ handling may lead to the overestimation of minimum population size, particularly in instances where the PIP-TAZ bactericidal effect suppressed the bacterial population below the quantifiable limit. Consequently, this approach might introduce additional bias into the estimation of the first-order mutation rate constant ($k_{transfer}$), especially at higher PIP-TAZ concentrations where measurement values fell below the LLoQ. While our sensitivity analysis demonstrates the impact of deviation in $k_{transfer}$ value towards model prediction was found to relatively limited compared to other literature-derived parameters (Fig. S7), future studies may explore more advanced BLoQ handling methods, such as those similar to methods M3 or M4 implemented in NONMEM[35], as potential approaches for handling BLoQ in the analysis of STK experiment data.

Exploring the efficiency of different PIP-TAZ concertation ranges

The following simulations were performed to explore and evaluate the efficiency of PIP-TAZ concentration ranges beyond its commonly applied 8:1 dosing ratio[4] (**Fig. 4**, Fig. S8). The simulations were performed using the porin down-regulation and efflux pump up-regulation models, the two key resistance mechanisms identified in the previous step. The expected area of inhibitory PIP-TAZ ranges varied depending on the underlying resistance mechanism. This area of 24-hours growth inhibition was defined as the concentrations in which the growth of the strain was inhibited to a level that population size observed at the 24^{th} hours was less than its size in the beginning of the simulation.

By overlapping the ranges of inhibitory PIP-TAZ concentrations derived from each resistance models, our analysis determined the range of PIP-TAZ concentrations that are expected to suppress the growth of the susceptible as well as the resistant bacterial subpopulations, irrespective of the underlying resistance mechanism (**Fig. 4**, double-shaded area). This suggested the possibility to select specific PIP-TAZ doses that impede bacterial growth even if resistance development occurred during treatment. Notably, the range of inhibitory PIP-TAZ concentrations identified in this exercise represents a space of concentrations that is not bound to the widely used 8:1 dose ratio of PIP:TAZ[4]. It may thus be beneficial for future studies to explore and optimize PIP-TAZ doses without the constraint of the currently used 8:1 dose ratio.

Discussion

Understanding the individual impact of different resistance mechanisms offers critical information to identify systems that hold the most potential as pharmacological tar-

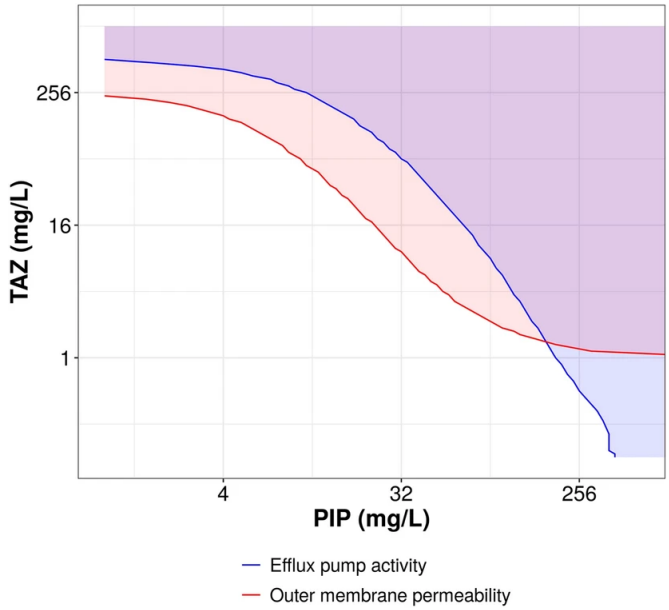

Fig. 4 | Model-predicted PIP-TAZ concentration range for achieving growth inhibition. Predicted PIP-TAZ concentration range to inhibit the growth of CTX-M-15-producing *K. pneumoniae* based on the underlying resistance mechanism. Simulations were performed using the porin down-regulation and efflux pump up-regulation models with an initial population size of 10^5 CFU/mL. Shaded area represents the range of PIP-TAZ concentrations where growth inhibition at 24 hours was expected for the specific resistance mechanism.

gets to counter the development of antibiotic resistance[15,32]. The current study demonstrated how semi-mechanistic models can be used to identify critical PIP-TAZ resistance mechanisms based on an STK experiment. Here, several semi-mechanistic models were developed to individually explore the potential involvement of specific mechanisms in reducing periplasmic PIP-TAZ concentration. Our analysis explored the extent in which changes in porin, efflux pump, and β-lactamase expression and functional capability may mediate PIP-TAZ resistance in a CTX-M-15-producing *K. pneumoniae* strain (**Fig. 1**).

Our analysis identified porin down-regulation and efflux pump up-regulation as potential key mediators of PIP-TAZ resistance. Our in-silico findings agree with previous experimental studies performed in a similar setting that underlined the importance of porin loss and increase in efflux pump activity in mediating BL-BLI resistance[26,27]. Unlike changes in β-lactamase activity, changes in porin and efflux pump activities are often seen as a minor concurrence to β-lactamase-related resistance mechanisms[34]. In contrast to this view, our analysis showed that the two resistance mechanisms are individually capable of conveying the observed extent of PIP-TAZ resistance. Notably, the regulation of porin[36] and efflux pump[37] expression also play a key role in controlling the osmolarity of a bacterial cell. Regulatory network controlling the expression of porin and efflux pumps are thus present in most – if not all – Gram-negative bacteria[38]. Knowing the important role of osmotic pressure during BL-induced cell lysis[39], it can be hypothesized that the same network of porin and efflux pump regulation, as well as mutational events associated with the network, is triggered when the cell is exposed to PIP-TAZ. Subsequently, this network of porin and efflux pump regulation may provide

a path to resistance that is likely to be shared among Gram-negative bacteria.

Although the current study highlighted two single-event mechanisms as key mechanisms to PIP-TAZ resistance, these mechanisms may occur alongside other resistance mechanisms. For example, previous studies revealed how a decrease in outer membrane permeability can coincide with altered β-lactamase activity in a single *K. pneumoniae* strain[40]. These reports hinted the potential value of a model that can simultaneously explore multiple resistance mechanisms, although additional measurement on the specific resistant mechanism might be needed to maintain the certainty of the parameter estimates. Our analysis did not exclude the potential contribution of resistance mechanisms beyond porin loss and efflux pump up-regulation. Previous studies also associated the remaining resistance mechanisms to resistant phenotypes against BL-type antibiotics with or without BLI pairing in bacteremia (**Table 3**). However, the extent of cellular changes estimated in our models for the remaining 11 resistance mechanisms could not be supported by past experimental observation. This suggested the unlikely role of these mechanisms as a sole driver of PIP-TAZ resistance as observed in our experiment.

Our analysis also utilized porin down-regulation and efflux pump up-regulation models to explore how different these two mechanisms may impact the expected bacterial growth at a higher PIP-TAZ concentration (**Fig. 4**, Fig. S8). In this context, our models were used as a learning tool to explore the effectiveness of PIP-TAZ doses beyond its generally applied 8:1 dosing ratio[4]. Consequently, this opened the possibility for future studies to attempt further optimization of PIP-TAZ doses in anticipation of a specific resistance mechanism while considering the safety limits of PIP-TAZ dosing[41].

Mathematical models represent simplifications of more complex (biological) phenomena. Such simplification can be necessary to describe events that are not well characterized and to derive a more generalized representation of cellular events. Nevertheless, the exclusion of some details may lead to loss of potentially important information. In our models, drug influx through porins were simplified into a single diffusion model despite the presence of multiple porin subtypes in *K. pneumoniae*[26,33]. This simplification prevented us from identifying a specific porin subtype that may be the most prevalent in conveying resistance to PIP-TAZ. Similarly, the binding of PIP to different PBP variants and its associated bactericidal effect was simplified into an empirical concentration-effect equation (**Eq. 7**). This prevented us from using the model to explore PBP-related resistance mechanisms. Nevertheless, the empirical simplification of drug effect was necessary due to the limited information on PIP interaction with different PBP variants and the consequence of this interaction on the resulting bactericidal effect. While a more detailed mechanistic model can be superior in describing a complex biological event, over-extending model complexity, for example by implementing PBP interactions with PIP-TAZ without sufficient data to support such an interaction, may impair the certainty of the resulting parameter estimates[42]. Additional studies to determine the dynamics of these interactions are thus needed to build a more detailed model. Our model also simplified the development of resistant bacterial sub-population using a first-order kinetics (**Eqs. 9 − 10**). Thus, the development of resistance was depicted as a stepwise event. Consequently, the models were unable to depict neither gradual nor dose-responsive development of resistance. This limitation may, in part, explain the predictive inaccuracies during regrowth events at higher PIP-TAZ concentrations despite the relatively more accurate prediction observed at lower PIP-TAZ concentrations (**Fig. 3**).

The semi-mechanistic models presented in this study were partly developed using bioanalytical information adopted from other bacterial species and strains. This decision

was made due to the unavailability of PIP-TAZ and *K. pneumoniae*-specific parameter values at the time of the study. Considering the potential differences in these system-specific characteristics, the incorporation of PIP-TAZ and *K. pneumoniae*-specific parameters may prove beneficial for future efforts to enhance the descriptive and predictive capabilities of the semi-mechanistic model. Therefore, future studies may focus on investigating these mechanisms to further characterize PIP-TAZ resistance in *K. pneumoniae*.

Conclusion

The current study presents a semi-mechanistic modeling workflow and its application to complement experimental studies on antimicrobial pharmacodynamics and resistance. Our model-based analysis highlighted porin down-regulation and efflux pump up-regulation as potential mediators of PIP-TAZ resistance and suggested the importance of these mechanisms as prospective focus for future efforts to explore strategies against PIP-TAZ resistance. Moreover, we showed how the models can be used to evaluate PIP-TAZ concentration ranges for suppressing bacterial growth during resistance emergence. In conclusion, our study demonstrated the utility of semi-mechanistic models in complementing experimental efforts to provide insight into the relative impact of potential resistance mechanisms on antibiotic treatment response, help guide subsequent experimental designs, and support the rational design of antibiotic treatment to against resistance development.

References

1. Oliphant, C. M., & Eroschenko, K. (2015). Antibiotic Resistance, Part 2: Gram-negative Pathogens. *The Journal for Nurse Practitioners*, *11*(1), 79–86. https://doi.org/10.1016/j.nurpra.2014.10.008
2. Dhillon, R. H.-P., & Clark, J. (2012). Esbls: A Clear and Present Danger? *Critical Care Research and Practice*, *2012*, 625170. https://doi.org/10.1155/2012/625170
3. Drawz, S. M., & Bonomo, R. A. (2010). Three decades of beta-lactamase inhibitors. *Clinical Microbiology Reviews*, *23*(1), 160–201. https://doi.org/10.1128/CMR.00037-09
4. Abodakpi, H., Chang, K.-T., Gao, S., Sánchez-Díaz, A. M., Cantón, R., & Tam, V. H. (2019). Optimal Piperacillin-Tazobactam Dosing Strategies against Extended-Spectrum-β-Lactamase-Producing Enterobacteriaceae. *Antimicrobial Agents and Chemotherapy*, *63*(2), e01906–18. https://doi.org/10.1128/AAC.01906-18
5. Abdelraouf, K., Chavda, K. D., Satlin, M. J., Jenkins, S. G., Kreiswirth, B. N., & Nicolau, D. P. (2020). Piperacillin-Tazobactam-Resistant/Third-Generation Cephalosporin-Susceptible Escherichia coli and Klebsiella pneumoniae Isolates: Resistance Mechanisms and In vitro-In vivo Discordance. *International Journal of Antimicrobial Agents*, *55*(3), 105885. https://doi.org/10.1016/j.ijantimicag.2020.105885
6. Zhou, K., Tao, Y., Han, L., Ni, Y., & Sun, J. (2019). Piperacillin-Tazobactam (TZP) Resistance in Escherichia coli Due to Hyperproduction of TEM-1 β-Lactamase Mediated by the Promoter Pa/Pb. *Frontiers in Microbiology*, *10*, 833. https://doi.org/10.3389/fmicb.2019.00833
7. Nicolas-Chanoine, M.-H., Mayer, N., Guyot, K., Dumont, E., & Pagès, J.-M. (2018). Interplay Between Membrane Permeability and Enzymatic Barrier Leads to Antibiotic-Dependent Resistance in Klebsiella Pneumoniae. *Frontiers in Microbiology*, *9*, 1422. https://doi.org/10.3389/fmicb.2018.01422
8. Fernández, L., & Hancock, R. E. W. (2012). Adaptive and mutational resistance: Role of porins and efflux pumps in drug resistance. *Clinical Microbiology Reviews*, *25*(4), 661–681. https://doi.org/10.1128/CMR.00043-12
9. Pages, J.-M., Lavigne, J.-P., Leflon-Guibout, V., Marcon, E., Bert, F., Noussair, L., & Nicolas-Chanoine, M.-H. (2009). Efflux pump, the masked side of beta-lactam resistance in Klebsiella pneumoniae clinical isolates. *PloS One*, *4*(3), e4817. https://doi.org/10.1371/journal.pone.0004817

10. Kakoullis, L., Papachristodoulou, E., Chra, P., & Panos, G. (2021). Mechanisms of Antibiotic Resistance in Important Gram-Positive and Gram-Negative Pathogens and Novel Antibiotic Solutions. *Antibiotics*, *10*(4), 415. https://doi.org/10.3390/antibiotics10040415
11. Heinz, E., Ejaz, H., Bartholdson Scott, J., Wang, N., Gujaran, S., Pickard, D., Wilksch, J., Cao, H., Haq, I.-U., Dougan, G., & Strugnell, R. A. (2019). Resistance mechanisms and population structure of highly drug resistant Klebsiella in Pakistan during the introduction of the carbapenemase NDM-1. *Scientific Reports*, *9*(1), 2392. https://doi.org/10.1038/s41598-019-38943-7
12. Masi, M., Réfregiers, M., Pos, K. M., & Pagès, J.-M. (2017). Mechanisms of envelope permeability and antibiotic influx and efflux in Gram-negative bacteria. *Nature Microbiology*, *2*, 17001. https://doi.org/10.1038/nmicrobiol.2017.1
13. Prochnow, H., Fetz, V., Hotop, S.-K., García-Rivera, M. A., Heumann, A., & Brönstrup, M. (2019). Subcellular Quantification of Uptake in Gram-Negative Bacteria. *Analytical Chemistry*, *91*(3), 1863–1872. https://doi.org/10.1021/acs.analchem.8b03586
14. Mi, K., Zhou, K., Sun, L., Hou, Y., Ma, W., Xu, X., Huo, M., Liu, Z., & Huang, L. (2022). Application of Semi-Mechanistic Pharmacokinetic and Pharmacodynamic Model in Antimicrobial Resistance. *Pharmaceutics*, *14*(2), 246. https://doi.org/10.3390/pharmaceutics14020246
15. Sahoo, S., Mishra, A., Kaur, H., Hari, K., Muralidharan, S., Mandal, S., & Jolly, M. K. (2021). A mechanistic model captures the emergence and implications of non-genetic heterogeneity and reversible drug resistance in ER+ breast cancer cells. *NAR cancer*, *3*(3), zcab027. https://doi.org/10.1093/narcan/zcab027
16. Liakopoulos, A., Betts, J., La Ragione, R., van Essen-Zandbergen, A., Ceccarelli, D., Petinaki, E., Koutinas, C. K., & Mevius, D. J. (2018). Occurrence and characterization of extended-spectrum cephalosporin-resistant Enterobacteriaceae in healthy household dogs in Greece. *Journal of Medical Microbiology*, *67*(7), 931–935. https://doi.org/10.1099/jmm.0.000768
17. Kojima, S., & Nikaido, H. (2013). Permeation rates of penicillins indicate that Escherichia coli porins function principally as nonspecific channels. *Proceedings of the National Academy of Sciences of the United States of America*, *110*(28), E2629–2634. https://doi.org/10.1073/pnas.1310333110
18. Lim, S. P., & Nikaido, H. (2010). Kinetic parameters of efflux of penicillins by the multidrug efflux transporter AcrAB-TolC of Escherichia coli. *Antimicrobial Agents and Chemotherapy*, *54*(5), 1800–1806. https://doi.org/10.1128/AAC.01714-09
19. Faheem, M., Rehman, M. T., Danishuddin, M., & Khan, A. U. (2013). Biochemical characterization of CTX-M-15 from Enterobacter cloacae and designing a novel non-β-lactam-β-lactamase inhibitor. *PloS One*, *8*(2), e56926. https://doi.org/10.1371/journal.pone.0056926
20. Helfand, M. S., Bethel, C. R., Hujer, A. M., Hujer, K. M., Anderson, V. E., & Bonomo, R. A. (2003). Understanding resistance to beta-lactams and beta-lactamase inhibitors in the SHV beta-lactamase: Lessons from the mutagenesis of SER-130. *The Journal of Biological Chemistry*, *278*(52), 52724–52729. https://doi.org/10.1074/jbc.M306059200
21. Mr, M. (1992). Proteases and protein degradation in Escherichia coli. *Experientia*, *48*(2). https://doi.org/10.1007/BF01923511
22. Perilli, M., Franceschini, N., Bonfiglio, G., Segatore, B., Stefani, S., Nicoletti, G., Perez, M. M., Bianchi, C., Zollo, A., & Amicosante, G. (2000). A kinetic study on the interaction between tazobactam (a penicillanic acid sulphone derivative) and active-site serine beta-lactamases. *Journal of Enzyme Inhibition*, *15*(1), 1–10.
23. Nielsen, E. I., & Friberg, L. E. (2013). Pharmacokinetic-pharmacodynamic modeling of antibacterial drugs. *Pharmacological Reviews*, *65*(3), 1053–1090. https://doi.org/10.1124/pr.111.005769
24. Viaene, E., Chanteux, H., Servais, H., Mingeot-Leclercq, M.-P., & Tulkens, P. M. (2002). Comparative Stability Studies of Antipseudomonal β-Lactams for Potential Administration through Portable Elastomeric Pumps (Home Therapy for Cystic Fibrosis Patients) and Motor-Operated Syringes (Intensive Care Units). *Antimicrobial Agents and Chemotherapy*, *46*(8), 2327–2332. https://doi.org/10.1128/aac.46.8.2327-2332.2002
25. Samara, E., Moriarty, T. F., Decosterd, L. A., Richards, R. G., Gautier, E., & Wahl, P. (2017). Antibiotic stability over six weeks in aqueous solution at body temperature with and without heat treatment that mimics the curing of bone cement. *Bone & Joint Research*, *6*(5), 296–306. https://doi.org/10.1302/2046-3758.65.BJR-2017-0276.R1
26. Kaczmarek, F. M., Dib-Hajj, F., Shang, W., & Gootz, T. D. (2006). High-level carbapenem resistance in a Klebsiella pneumoniae clinical isolate is due to the combination of bla(ACT-1) beta-lactamase production, porin OmpK35/36 insertional inactivation, and down-regulation of the phosphate transport porin phoe. *Antimicrobial Agents and Chemotherapy*, *50*(10), 3396–3406. https://doi.org/10.1128/AAC.00285-06
27. Lee, Y.-J., Huang, C.-H., Ilsan, N. A., Lee, I.-H., & Huang, T.-W. (2021). Molecular Epidemiology and Characterization of Carbapenem-Resistant Klebsiella pneumoniae Isolated from Urine at a

Teaching Hospital in Taiwan. *Microorganisms*, *9*(2), 271. https://doi.org/10.3390/microorganisms9020271
28. Singh, T., Singh, P. K., Das, S., Wani, S., Jawed, A., & Dar, S. A. (2019). Transcriptome analysis of beta-lactamase genes in diarrheagenic Escherichia coli. *Scientific Reports*, *9*(1), 3626. https://doi.org/10.1038/s41598-019-40279-1
29. Jones, A. K., Ranjitkar, S., Lopez, S., Li, C., Blais, J., Reck, F., & Dean, C. R. (2018). Impact of Inducible blaDHA-1 on Susceptibility of Klebsiella pneumoniae Clinical Isolates to LYS228 and Identification of Chromosomal mpl and ampD Mutations Mediating Upregulation of Plasmid-Borne blaDHA-1 Expression. *Antimicrobial Agents and Chemotherapy*, *62*(10), e01202–18. https://doi.org/10.1128/AAC.01202-18
30. Wang, X., Minasov, G., & Shoichet, B. K. (2002). Evolution of an antibiotic resistance enzyme constrained by stability and activity trade-offs. *Journal of Molecular Biology*, *320*(1), 85–95. https://doi.org/10.1016/S0022-2836(02)00400-X
31. Ramdani-Bouguessa, N., Manageiro, V., Jones-Dias, D., Ferreira, E., Tazir, M., & Caniça, M. (2011). Role of SHV β-lactamase variants in resistance of clinical Klebsiella pneumoniae strains to β-lactams in an Algerian hospital. *Journal of Medical Microbiology*, *60*(Pt 7), 983–987. https://doi.org/10.1099/jmm.0.030577-0
32. Clegg, L. E., & Mac Gabhann, F. (2015). Molecular Mechanism Matters: Benefits of mechanistic computational models for drug development. *Pharmacological research*, *99*, 149–154. https://doi.org/10.1016/j.phrs.2015.06.002
33. Tsai, Y.-K., Fung, C.-P., Lin, J.-C., Chen, J.-H., Chang, F.-Y., Chen, T.-L., & Siu, L. K. (2011). Klebsiella pneumoniae outer membrane porins OmpK35 and OmpK36 play roles in both antimicrobial resistance and virulence. *Antimicrobial Agents and Chemotherapy*, *55*(4), 1485–1493. https://doi.org/10.1128/AAC.01275-10
34. Maurya, N., Jangra, M., Tambat, R., & Nandanwar, H. (2019). Alliance of Efflux Pumps with β-Lactamases in Multidrug-Resistant Klebsiella pneumoniae Isolates. *Microbial Drug Resistance*, *25*(8), 1155–1163. https://doi.org/10.1089/mdr.2018.0414
35. Bergstrand, M., & Karlsson, M. O. (2009). Handling data below the limit of quantification in mixed effect models. *The AAPS journal*, *11*(2), 371–380. https://doi.org/10.1208/s12248-009-9112-5
36. Graeme-Cook, K. A. (1991). The regulation of porin expression in Escherichia coli: Effect of turgor stress. *FEMS microbiology letters*, *63*(2-3), 219–223. https://doi.org/10.1016/0378-1097(91)90089-s
37. Zhu, M., & Dai, X. (2018). High Salt Cross-Protects Escherichia coli from Antibiotic Treatment through Increasing Efflux Pump Expression. *mSphere*, *3*(2), e00095–18. https://doi.org/10.1128/mSphere.00095-18
38. Ferrand, A., Vergalli, J., Pagès, J.-M., & Davin-Regli, A. (2020). An Intertwined Network of Regulation Controls Membrane Permeability Including Drug Influx and Efflux in Enterobacteriaceae. *Microorganisms*, *8*(6), 833. https://doi.org/10.3390/microorganisms8060833
39. Wong, F., Wilson, S., Helbig, R., Hegde, S., Aftenieva, O., Zheng, H., Liu, C., Pilizota, T., Garner, E. C., Amir, A., & Renner, L. D. (2021). Understanding Beta-Lactam-Induced Lysis at the Single-Cell Level. *Frontiers in Microbiology*, *12*, 712007. https://doi.org/10.3389/fmicb.2021.712007
40. Khalifa, S. M., Abd El-Aziz, A. M., Hassan, R., & Abdelmegeed, E. S. (2021). β-lactam resistance associated with β-lactamase production and porin alteration in clinical isolates of E. coli and K. pneumoniae. *PloS One*, *16*(5), e0251594. https://doi.org/10.1371/journal.pone.0251594
41. Kim, M. K., Xuan, D., Quintiliani, R., Nightingale, C. H., & Nicolau, D. P. (2001). Pharmacokinetic and pharmacodynamic profile of high dose extended interval piperacillin-tazobactam. *The Journal of Antimicrobial Chemotherapy*, *48*(2), 259–267. https://doi.org/10.1093/jac/48.2.259
42. Sher, A., Niederer, S. A., Mirams, G. R., Kirpichnikova, A., Allen, R., Pathmanathan, P., Gavaghan, D. J., van der Graaf, P. H., & Noble, D. (2022). A Quantitative Systems Pharmacology Perspective on the Importance of Parameter Identifiability. *Bulletin of Mathematical Biology*, *84*(3), 39. https://doi.org/10.1007/s11538-021-00982-5

Supplementary Materials

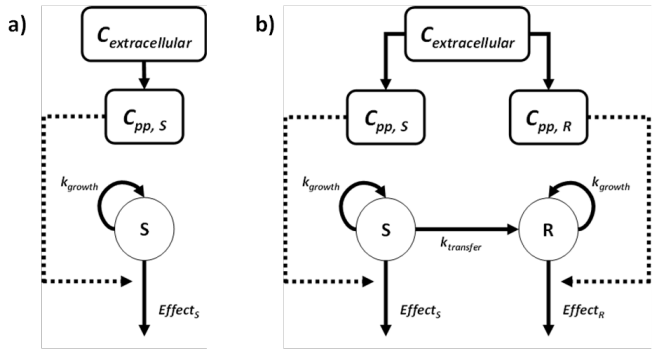

Fig. S1 | One- and two-population growth model. The current study used one- and two-population growth models to describe the behavior of the observed *Klebsiella pneumoniae* strain in different concentrations of PIP-TAZ. **a)** The one-population model assumed that the bacterial population consists of a single population and was used to describe the growth of the strain before the onset of regrowth. **b)** The two-population model assumed the presence of two bacterial sub-populations and was used to empirically describe the development of resistance. The size of the R sub-population was assumed to be zero at the start of the experiment. The first-order transfer rate from the sensitive (S) to the resistant (R) subpopulation was assumed to be unidirectional.

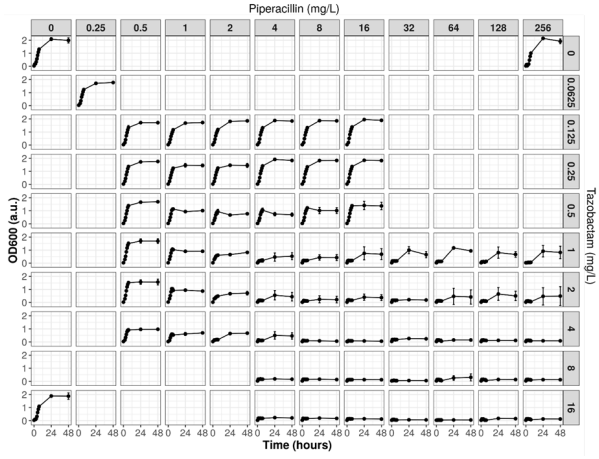

Fig. S2 | *Preliminary screening of Klebsiella pneumoniae GR116.26 in different PIP-TAZ concentration in a checkerboard setup.* Concentration of the bacterial population was shown as optical density at 600 nm (OD_{600}). Absence of either PIP or TAZ eliminated bactericidal effect, even at a high concentration of the other drug. Increasing concentration of PIP and TAZ lead to a higher suppression of bacterial growth. Each data point represented the mean of three replicate measurements. Error bars represented the standard deviation of the triplicate measurements.

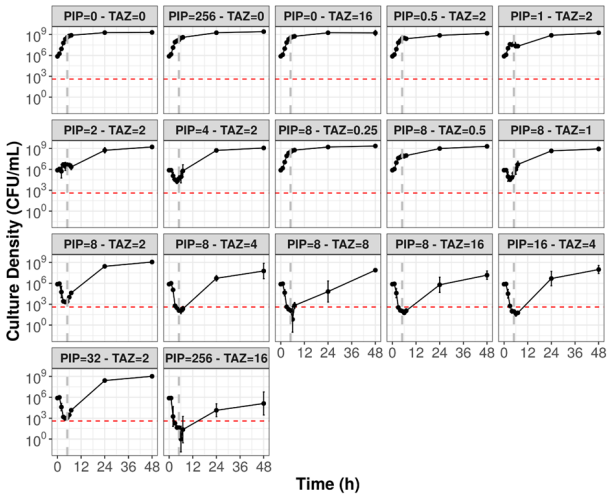

Fig. S3 | Growth behavior of CTX-M-15-producing *Klebsiella pneumoniae* in different concentrations of PIP-TAZ. Initial decrease in population size was observable at higher concentrations of PIP-TAZ. An initial decrease of population size was always followed by population regrowth, which became prominent after the 5th hour (grey dashed line). Red dashed line represents LLOQ of the measurement method. Data points represent mean of three measurement replicates. Error bars represented mean ± standard deviation of the three replicate measurements.

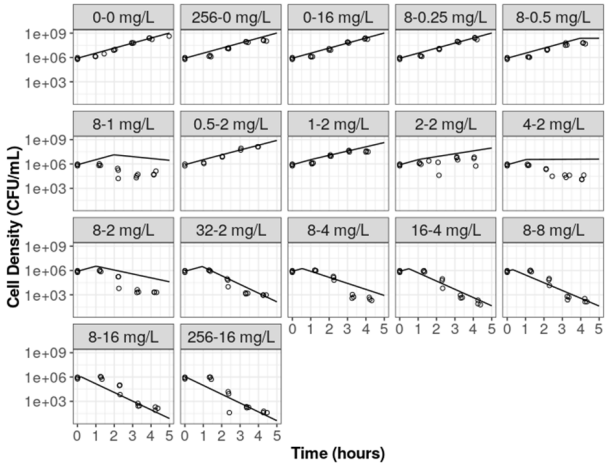

Fig. S4 | *Klebsiella pneumoniae* GR116.26 growth in static PIP-TAZ concentration before the onset of regrowth. Concentration of the bacterial population was measured as concentration of colony forming units. Absence of either PIP or TAZ eliminates bactericidal effect, even at a high concentration of the other drug. Increasing concentration of PIP and TAZ lead to a higher suppression of bacterial growth. Solid lines represented the model prediction of the population growth at each assay condition. Measurement triplicates were showed as individual data points.

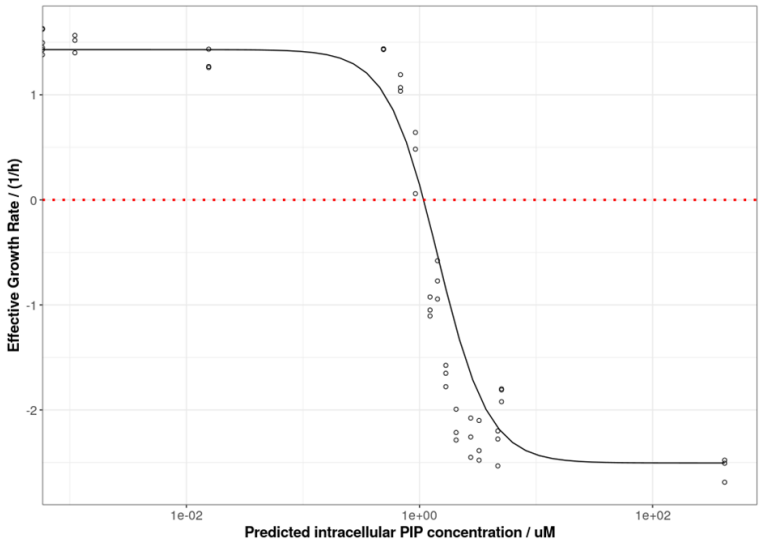

Fig. S5 | Concentration-effect relationship between bacterial growth and predicted periplasmic PIP concentration. Periplasmic PIP concentration was predicted using the one-population model. The effective (observed) growth rate of the strain in the first 5 hours of the experiment at different PIP-TAZ concentrations were mapped its respective predicted periplasmic PIP concentration. Effective growth rate for each experimental conditions and replicates were derived independently by log-linear regression. This was performed to confirm the applicability of our model to describe drug effect as a function of intracellular PIP concentration. Solid line indicated the concentration-effect curve predicted by the model. Red dashed line represented an effective growth rate of zero. Intercept between the solid line and the red dotted line indicated the point where intracellular concentration is high enough to exert a bactericidal effect that is equal to the maximum growth rate of the strain. The molecular mass of PIP was 516.5 g/mol.

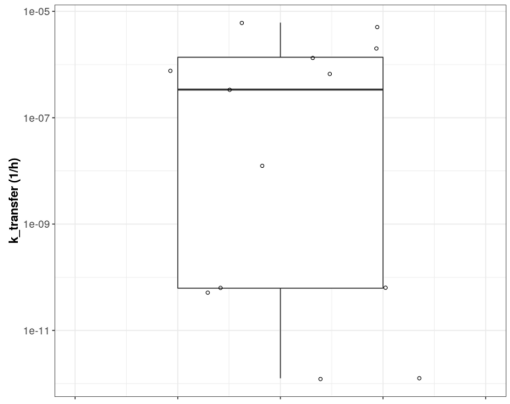

Fig. S6 | Estimated susceptible-to-resistant transfer rate constant differs in each resistance model. Data points represent individual ktransfer estimate for each resistant model.

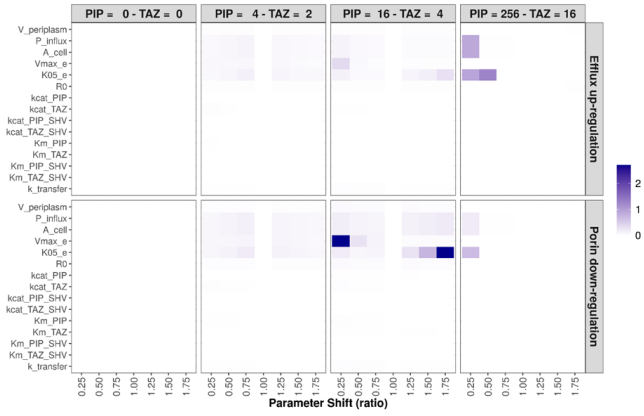

Fig. S7 | Parameter sensitivity analysis of literature-based parameters and first-order population transfer rate constant. Sensitivity analysis was performed on four selected PIP-TAZ concentrations to represent conditions with different observed bactericidal effects. The potential impact of ktransfer deviations to model prediction was compared with that of literature-based parameters. Absolute sensitivity coefficients were calculated by taking the absolute value of the ratio of the shift in total bacterial load (area under the bacterial growth curve) to the relative ratio of parameter shift. A darker blue color indicated a higher parameter sensitivity at the tested condition.

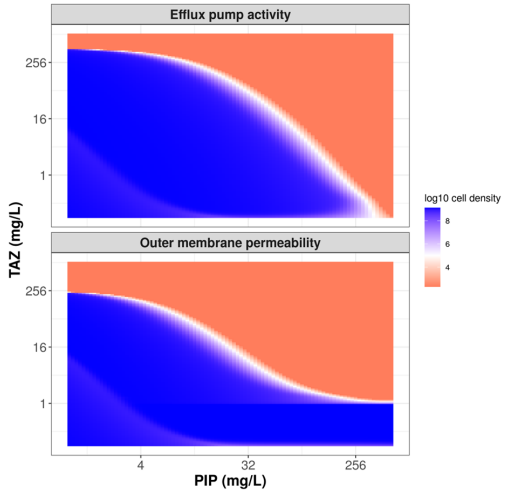

Fig. S8 | Simulated *Klebsiella pneumoniae* GR116.26 growth with different underlying resistance mechanisms. Simulations were performed using the porin down-regulation and efflux pump up-regulation models. Simulations were initiated with an initial population size of 105 CFU/mL. Color represents the cell density (in log10- CFU/mL) expected at the 24th hour. In general, blue and red indicated a PIP-TAZ concentration where cell density was higher and lower than that of the inoculum, respectively. White grids represented PIP-TAZ concentration where cell density is approximately equal to the inoculum.

Table S1. Assumptions made during the model development process

Assumption	Reference
Natural growth of the bacteria follows the population-limited growth model	[Ref. S1]
Bactericidal effect depends on the periplasmic PIP concentration	[4]
The bactericidal effect of TAZ is negligible	[4]
CTX-M-15 and SHV-1 have the same initial steady-state expression	–
TAZ acts as a suicide inhibitor, inactivating the β-lactamase that acts on TAZ by forming a stable acyl-enzyme complex.	[21]
Intrinsic β-lactamase turnover rate was similar to most intracellular proteins in *E. coli* at 1% per hour	[22]
PIP and TAZ binding to β-lactamase and efflux pumps are competitive	[19]
PIP and TAZ diffusion into the periplasm was governed by porin-facilitated passive diffusion	[17]
PIP–TAZ diffusion into the cytoplasm is negligible with respect to its influx	[17]
TAZ influx and efflux characteristics are equivalent to that of PIP	–

Ref. S1. Mouton, J. W., Vinks, A. A., & Punt, N. C. (1997). Pharmacokinetic-pharmacodynamic modeling of activity of ceftazidime during continuous and intermittent infusion. *Antimicrob. Agents Chemother.*, 41(4), 733–738. https://doi.org/10.1128/AAC.41.4.733

Table S2. Mean maximum efflux rate and permeability coefficient of β-lactams

Drug	Max. efflux rate (nmol/mg/s)	Permeability coefficient (μm/s)
Dicloxacillin	0.957	0.600
Cloxacillin	0.893	0.600
Oxacillin	0.993	0.600
Azlocillin	0.393	0.400
Mezlocillin	0.493	0.500
Piperacillin	0.383	0.367
Penicillin V	0.763	0.733
Ampicillin	0.373	0.800
Range	**0.373–0.993**	**0.367–0.800**

Value represents the mean of three replicate measurements reported by Lim and Nikaido, 2010 [18].